Available online at www.sciencedirect.com
SCIENCE DIRECT®
International Journal of Mass Spectrometry 233 (2004) 305–315
International Journal of Mass Spectrometry
www.elsevier.com/locate/ijms

Destruction of hydrocarbons in non-thermal, ambient-pressure, capillary discharge plasmas

A. Koutsospyros [a,b], S.-M. Yin [a,c,d], C. Christodoulatos [a,d], K. Becker [a,e,*]

[a] *Center for Environmental Systems, Stevens Institute of Technology, Hoboken, NJ 07030, USA*
[b] *Department of Civil and Environmental Engineering, University of New Haven, New Haven, CT 06516, USA*
[c] *PlasmaSol Corporation, Hoboken, NJ 07030, USA*
[d] *Department of Civil, Environmental, and Ocean Engineering, Stevens Institute of Technology, Hoboken, NJ 07030, USA*
[e] *Department of Physic and Engineering Physics, Stevens Institute of Technology, Hoboken, NJ 07030, USA*

Received 1 December 2003; accepted 30 December 2003

Abstract

This present work investigates the effectiveness of non-thermal diffuse plasmas for the destruction of environmental contaminants that are present in trace concentrations in respirable atmospheres. Parametric studies were carried out using three atmospheric-pressure capillary plasma reactors of varying geometry. Volatile aliphatic and aromatic hydrocarbons, at concentrations of up to several hundred parts per million (ppm), were used as prototypical compounds for these studies. Parameters studied included the reactor volume, the species residence time, the specific energy input, and the influent contaminant concentration. Moreover, the dependence of the overall destruction efficiency on specific energy, contaminant type, and presence of other contaminants in well-defined contaminant mixtures was evaluated. By-product formation during the plasma chemical destruction was assessed by monitoring the concentration of gaseous nitrogen and carbon oxides, namely, NO_x (NO, NO_2) and CO_x (CO, CO_2). Carbon mass balances were used to assess the possibility of complete contaminant destruction leading to mineralization. Systematic trends are highlighted and show that the destruction efficiency increases with specific energy, but tends to level off at values of specific energy that are compound dependent. An inverse relationship between the maximum destruction efficiency of a particular compound and its ionization energy was found for chemically similar compounds.

Keywords: Non-thermal plasma; Capillary plasma; Volatile organic compounds (VOC); Aromatic and aliphatic hydrocarbons

1. Introduction

Air regeneration and contaminant control are important issues in spacecraft and space station life support systems for maintaining a habitable crew cabin environment. Conventional technologies, such as particulate filters, activated carbon beds, chemisorbent beds, and catalytic oxidizers, suffer from limitations associated with the need for frequent regeneration and high mass, space, and/or energy requirements. Non-thermal plasmas can be a cost-effective and efficient alternative in reducing volatile organic compounds (VOCs) from a variety of sources. The utility of non-thermal plasmas for the treatment of various gaseous (non-substituted and substituted) aliphatic contaminant streams has been known for over a decade [1,2]. Electron impact dissociation and ionization appear to be the major pathways facilitating the destruction of organic compounds in dry environments, supplemented by electron attachment in the presence of moisture [3]. The destruction of VOCs proceeds homolytically via their excited states and has been found to be roughly inversely proportional to the ionization energy within a given class of compounds [4].

Very high plasma destruction rates are reported in the literature for various VOCs, namely, 100, 95, and 67% for toluene, methylene chloride, and CFC-113, respectively, using an ac powered ferroelectric packed-bed reactor (with $BaTiO_3$ pellets) [5]. Several studies investigated the influence of the plasma properties and reactor operating parameters on the destruction efficiency of organic compounds. In general, contaminant destruction efficiencies were found to increase with discharge current, species residence time, and initial VOC concentration [6]. The efficiency of the decomposition of benzene and the resulting by-product formation

* Corresponding author. Tel.: +1-201-216-5671.
E-mail address: kbecker@stevens.edu (K. Becker).

1387-3806/$ – see front matter © 2004 Elsevier B.V. All rights reserved.
doi:10.1016/j.ijms.2003.12.033

was studied in a ferroelectric pellet reactor as a function of packing material, pellet size, excitation frequency, initial VOC concentration, and background oxygen concentration [7]. Oda [8] observed destruction efficiencies in the range of 90–99% for VOCs, CFC-113, acetone, and isopropyl alcohol using a plasma induced by a surface discharge.

The performance of various plasma reactors, such as pulsed coronas, flow-stabilized coronas, and dielectric barrier discharges for treatment of organics, was reviewed by Urashima and Chang [9], Chang [10], and Futamura et al. [11]. Although considerable advances have been made in recent years, plasma reactors suffer from two major drawbacks: (a) corona and dielectric barrier sources in atmospheric-pressure air consist of filamentary plasma channels of very small effective volume requiring large-size reactors to achieve the desired contaminant residence times and (b) ambient-pressure, diffuse plasmas in air are difficult to generate and maintain requiring in some cases resistor banks that dissipate a significant amount of energy and/or require very high gas flow velocities for stabilization. In practice, these drawbacks translate to unfavorable power utilization and large footprint requirements.

In this paper, we present the results of the use of non-thermal, ambient-pressure diffuse plasmas generated in three plasma reactors based on the capillary plasma electrode (CPE) discharge concept [12,13] for the destruction of VOCs in gaseous streams. Results are presented for the destruction of prototypical aliphatic and aromatic VOCs. The dependence of the destruction efficiency on the particular reactor design as well as on operating parameters, such as power, specific energy, influent VOC concentration, species residence time, and by-product formation, was studied.

2. Experimental details

2.1. Overview

The experimental setup used in the work described herein consisted of three integrated sub-systems: (a) the feed gas mixing and delivery system, (b) the plasma reactor with its power source, and (c) the monitoring/analytical instrumentation for plasma diagnostics and characterization and for on-line analytical, qualitative/quantitative determination of the composition of the feed gas and effluent streams. A schematic diagram of the integrated setup is shown in Fig. 1. In the following sections we provide a description of the three reactor configurations used in our studies along with the analytical setup for the characterization of the treated gaseous streams. Some aspects of the setup have been described in earlier publications [14–16]. Briefly, a well-characterized mixture of atmospheric-pressure air and either *n*-heptane or toluene at concentrations of up to 700 parts per million (ppm) is fed into the plasma reactor which is powered by a high frequency (about 20 kHz), ac power supply. Discharge voltage, current, and power are continuously monitored during plasma operation. The plasma-treated gas stream leaving the reactor is analyzed using a variety of techniques and instruments including UV-Vis emission spectroscopy, UV-Vis spectrophotometry, FTIR spectroscopy, gas chromatography with mass spectrometry (GC-MS), gas chromatography with a thermal conductivity detector (GC-TCD), a Foxboro Miran 980 non-dispersed infrared (ND-IR) spectrophotometer, and an ENERAC 2000E Electrochemical Combustion Gas Analyzer for NO_x, CO, and CO_2.

2.2. Capillary plasma reactor configurations

2.2.1. The capillary plasma electrode (CPE) discharge concept

The basis for the atmospheric-pressure operation of the CPE discharge is a novel electrode design [12–15]. This design uses dielectric capillaries that cover one or both electrodes of a discharge device, which in many other aspects looks similar to a conventional dielectric barrier discharge, DBD [17]. However, the CPE discharge exhibits a mode of operation that is not observed in DBDs, the so-called "capillary jet mode". Here, the capillaries, with diameters in the range from 0.01 to 1 mm and length-to-diameter ratios of the order of 10:1, serve as plasma sources, which produce jets of high intensity plasma at atmospheric pressure under the right operating conditions. The plasma jets emerge from the end of the capillary and form a "plasma electrode" for the main discharge plasma. Under the right combination of capillary geometry, dielectric material, and exciting electric field, a stable uniform discharge can be achieved. The placement of the tubular dielectric capillary(s) in front of the electrode(s) is crucial for the development of the "capillary jet mode" of the CPE discharge. When the frequency reaches a critical value (which depends strongly on the *L*/*D* value and the feed gas), the capillaries "turn on" and a bright, intense plasma jet emerges from the capillaries. When many capillaries are placed in close proximity to each other, the emerging plasma jets overlap and the discharge appears uniform. This "capillary" mode is the preferred mode of operation and has been characterized in a rudimentary way for several laboratory-scale research discharge devices in terms of its characteristic electric and other properties [13–15,18–21]: peak discharge currents of up to 2 A, current density of up to 80 mA/cm^2, electron density n_e above 10^{12} cm^{-3}, power density of about 1.5 W/cm^3 in He and up to 20 W/cm^3 in air, and gas temperatures of 425–500 K in air. Using a Monte Carlo modeling code [22], the existence of the threshold frequency, which depends critically on the *L*/*D* ratio of the capillaries and dielectric material, has been verified [18,19]. The model also predicts relatively high average electron energies of 5–6 eV in the "capillary" mode.

While a full understanding of the fundamental processes in the CPE discharge on a microscopic scale has not been achieved, it appears that the capillaries act as individual high density plasma sources. The initial step is the formation of a

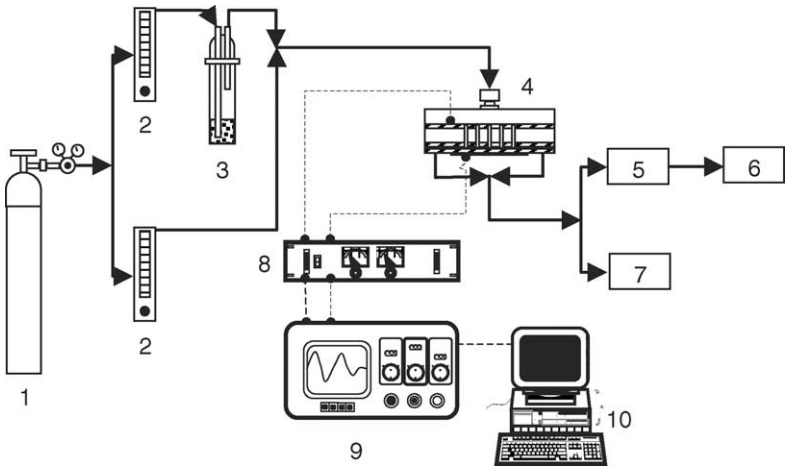

Fig. 1. Experimental setup of plasma reactor and analytical instruments for monitoring of contaminant destruction (1: compressed air; 2: flow rate controller; 3: VOC container; 4: plasma reactor; 5: gas chromatography-flame ionization detector; 6: NO_x, CO_x sensors; 7: Fourier transform-infrared spectrophotometer; 8: power supply; 9: oscilloscope; 10: personal computer running LabView).

streamer-like discharge inside each capillary, whose properties are critically determined by their interaction with the dielectric walls of the capillaries. In the following sections, we describe the three realizations of the CPE concept, which resulted in the different reactors employed in the present studies. The rationale for carrying out experiments using three different plasma reactor geometries and gas flow regimes based on the same CPE discharge plasma concept is twofold: (1) the first two reactors attempt to simulate the two extreme gas flow regimes (plug flow and completely mixed); (2) the third reactor design attempts to maximize the direct contact between the excited plasma species and the gas stream.

2.2.2. Annular plasma reactor (APR) with cylindrical electrodes

The first plasma reactor is an annular reactor designed to simulate plug flow conditions. The reactor body is made of Pyrex glass. The main components of the annular reactor are shown in Fig. 2. One of the electrodes consists of an aluminum screen that jackets the Pyrex glass cylinder, whereas the other electrode is made of an aluminum bar placed concentrically inside the glass cylinder surrounded by perforated alumina silicate dielectric material, Cotronics 902. Contaminated streams were fed axially into the reactor. This mode of operation allowed the contaminated gas stream to flow through the entire annulus of the reactor where exposure to the plasma occurred. The overall dimensions of the reactor were 254.0 mm in length with a 38.1 mm outer diameter. The spacing between the body and the dielectric was 2.38 mm resulting in an annular plasma volume of 21.1 cm^3. Thirteen rows of 12 equidistant capillaries of 1.59 mm diameter were drilled into the dielectric.

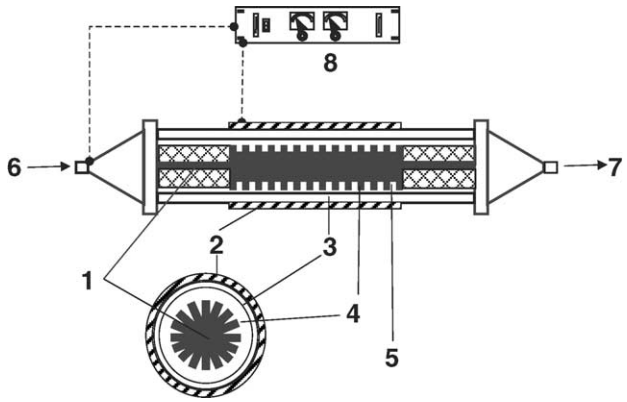

Fig. 2. Annular plasma reactor with cylindrical electrodes (1: aluminum bar electrode; 2: aluminum screen electrode; 3: dielectric material; 4: Pyrex glass body; 5: capillary; 6: gas inlet; 7: gas outlet; 8: power supply).

2.2.3. Rectangular plasma reactor with solid pin electrodes—cross-flow regime

The second reactor employs a multiple solid pin and plate configuration. The goal was to maximize contaminant exposure to the plasma and thus improve the energy efficiency. A schematic diagram of this reactor is shown in Fig. 3. The reactor consists of two parallel dielectric plates (304.8 mm by 152.4 mm), one of which is perforated with 0.4 mm

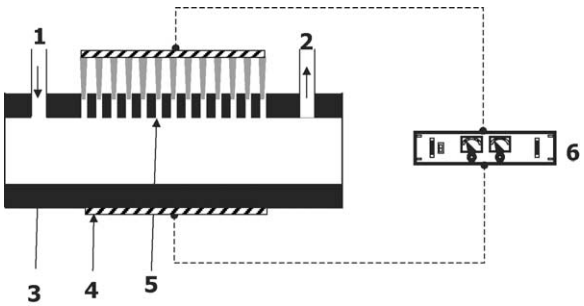

Fig. 3. Rectangular reactor configuration with solid pin capillary electrodes. The direction of the gas flow is perpendicular to the direction of the plasma jets, cross-flow geometry (1: gas inlet; 2: gas outlet; 3: dielectric material; 4: electrode; 5: capillary; 6: power supply).

diameter capillaries. The plates are separated forming a 3.18 or 1.59 mm gap through which the contaminated gas stream passed (cross-flow) and is treated by the plasma. The cathode consists of metallic pins, which are partially inserted into the capillary holes of the dielectric plate. The use of metallic pins minimizes energy losses in the system and improves plasma generation and stability. In addition, the pins eliminate destruction of the dielectric material caused by capacitive current breakthrough. The experiments were performed using a parallel plate pin electrode reactor with 100 capillaries and a working plasma volume of 49.24 or 24.62 cm^3 depending on the gap.

2.2.4. Rectangular plasma reactor with hollow pin electrodes—flow-through regime

The third plasma reactor was constructed by applying the following modifications to the previous reactor:

(i) The gas stream is introduced through the hollow pin electrodes and the capillaries, which aims to maximize the exposure of the contaminants to the region of highest plasma density. It was anticipated that this configuration will achieve a high degree of contaminant destruction at lower mean electron energies (which minimizes the production of undesirable by-products).
(ii) The reactor uses Pyrex glass plates instead of plastic, thus minimizing the generation of undesirable residues due to the interaction of the plasma with the reactor materials.
(iii) A hexagonal (instead of rectangular) pin arrangement guarantees equidistant plasma sources, which results in a more uniform plasma throughout the entire reactor volume.

The design employed a total of 37 pins, 0.79 mm diameter in an effort to minimize the development of a pressure drop when the gas flows through the hollow pin. Depending on the gap size between the two parallel plates (the two gap sizes used were 1.59 and 3.18 mm), the effective reactor volume was 3.44 and 6.81 cm^3, respectively (Fig. 4).

3. Results and discussion

In the following sub-sections, we report the results and basic findings of several parametric studies. In most of these studies, specific energy and contaminant destruction efficiency were chosen as the independent and dependent variable, respectively, with other operating variables serving as parameters. Although three variations of the CPE concept were used in the experiments, our results indicate that reactor geometry and flow regime seem to affect contaminant destruction efficiency only minimally. Nevertheless, the reactor type used is reported for each parametric study.

3.1. Effect of specific energy on contaminant destruction efficiency

The performance of the plasma reactors was evaluated by monitoring the contaminant destruction efficiency as a function of the specific energy. The contaminant destruction efficiency (E, %) is defined using the influent (C_o, ppm) and effluent (C, ppm) contaminant concentration:

$$E = \frac{C_o - C}{C_o} \times 100 \quad (1)$$

The specific energy (SE, J/cm^3), which is used as a measure of the energy expenditure of the plasma process, is defined using the input power (P, kW) and the gas flow rate entering the plasma reactor (Q, cm^3/s):

$$\mathrm{SE} = \frac{P}{Q} \quad (2)$$

The destruction efficiency of *n*-heptane in the APR is shown in Fig. 5, where the effluent *n*-heptane concentration and the destruction efficiency are plotted as a function of the specific energy (J/cm^3) for a fixed residence time of 0.60 s. The influent *n*-heptane concentration was around 700 ppm. The effluent *n*-heptane concentration decreases with increasing specific energy initially, while the destruction efficiency E at the same time increases. Both quantities reach a plateau of

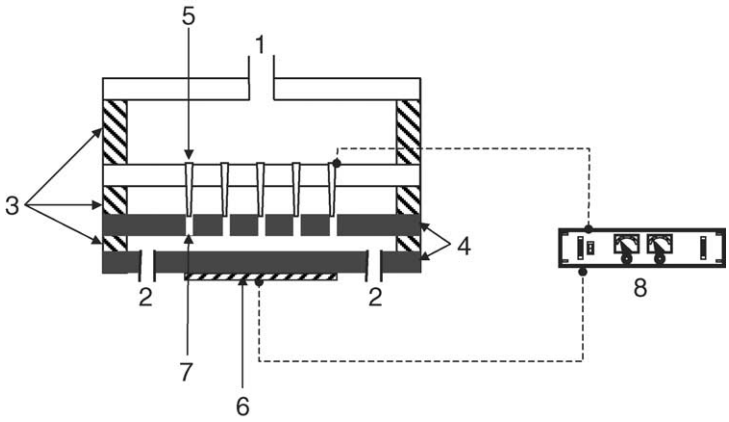

Fig. 4. Rectangular reactor with hollow pin capillary electrodes. The gas flows through the hollow pins, flow-through geometry (1: gas inlet; 2: gas outlet; 3: spacer; 4: dielectric material; 5: stainless steel hollow pins; 6: copper electrode; 7: capillary; 8: power supply).

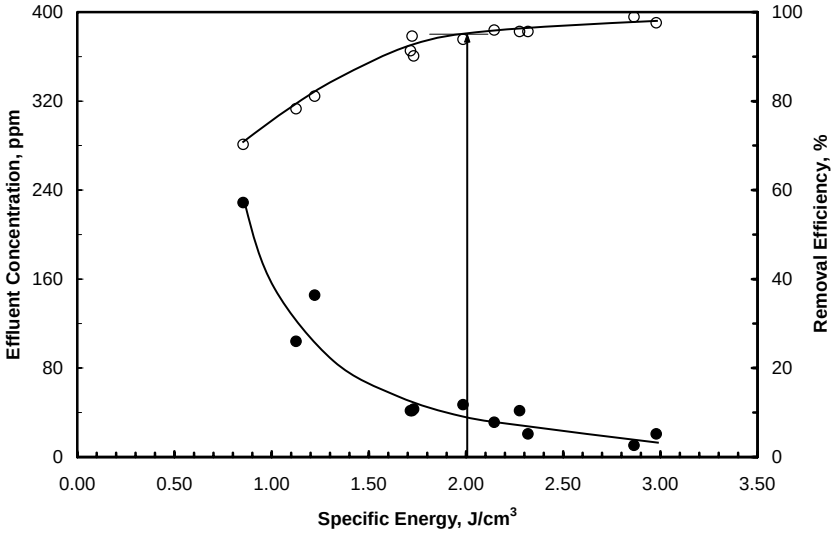

Fig. 5. Effluent contaminant concentration in ppm (solid circles) and destruction efficiency in % (open circles) for *n*-heptane treatment in the annular plasma reactor. The residence time was 0.6 s and the average influent concentration was 700 ppm. The vertical arrow indicates the value of the specific energy above which saturation in the destruction efficiency is achieved. The lines through the data points are just a guide to the eye.

about 80 ppm for the effluent *n*-heptane concentration and at about 95% for the destruction efficiency above a specific energy of 2 J/cm^3. This value of specific energy, where the destruction efficiency levels off for a particular contaminant, was found to depend slightly on the contaminant residence time.

The destruction of toluene follows a similar trend as shown in Fig. 6. For specific energy values exceeding 1.3 J/cm^3 and a contaminant residence time of 0.6 s, the ultimate toluene effluent concentration is approximately 100 ppm and the maximum destruction efficiency is about 80%. The influent toluene concentration was kept constant at 490 ppm for all experimental runs. Comparing the two contaminants, we find that a superior destruction efficiency is achieved for *n*-heptane (>95%) compared to toluene (∼80%). The required minimum energy at which these destruction efficiencies are realized is slightly higher for *n*-heptane (2.0 J/cm^3) compared to toluene (1.5 J/cm^3).

3.2. Effect of initial contaminant concentration

The effect of the influent contaminant concentration on the destruction efficiency was studied in the cross-flow reactor with the plasma generated in a multiple pin-to-plate configuration. Effluent concentration and destruction efficiencies for toluene are presented in Fig. 7 for three initial

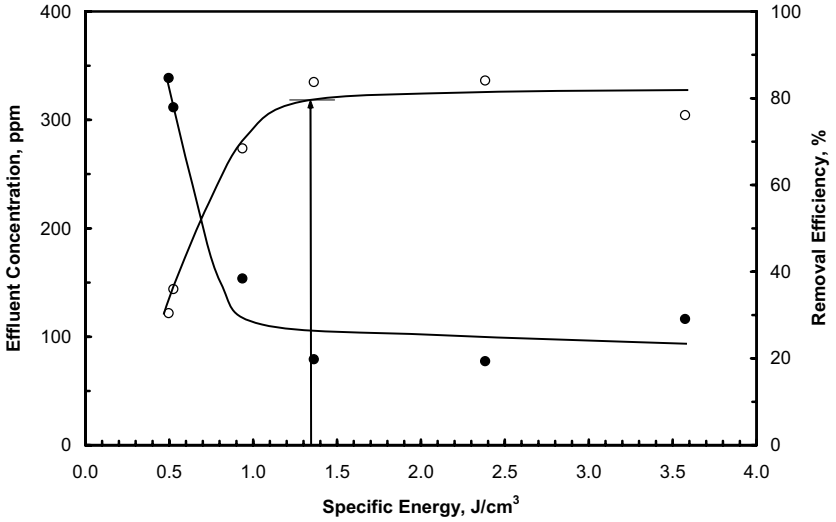

Fig. 6. Effluent contaminant concentration in ppm (solid circles) and destruction efficiency in % (open circles) for toluene treatment in the annular plasma reactor. The residence time was 0.6 s and the average influent concentration was 490 ppm. The vertical arrow indicates the value of the specific energy above which saturation in the destruction efficiency is achieved. The lines through the data points are just a guide to the eye.

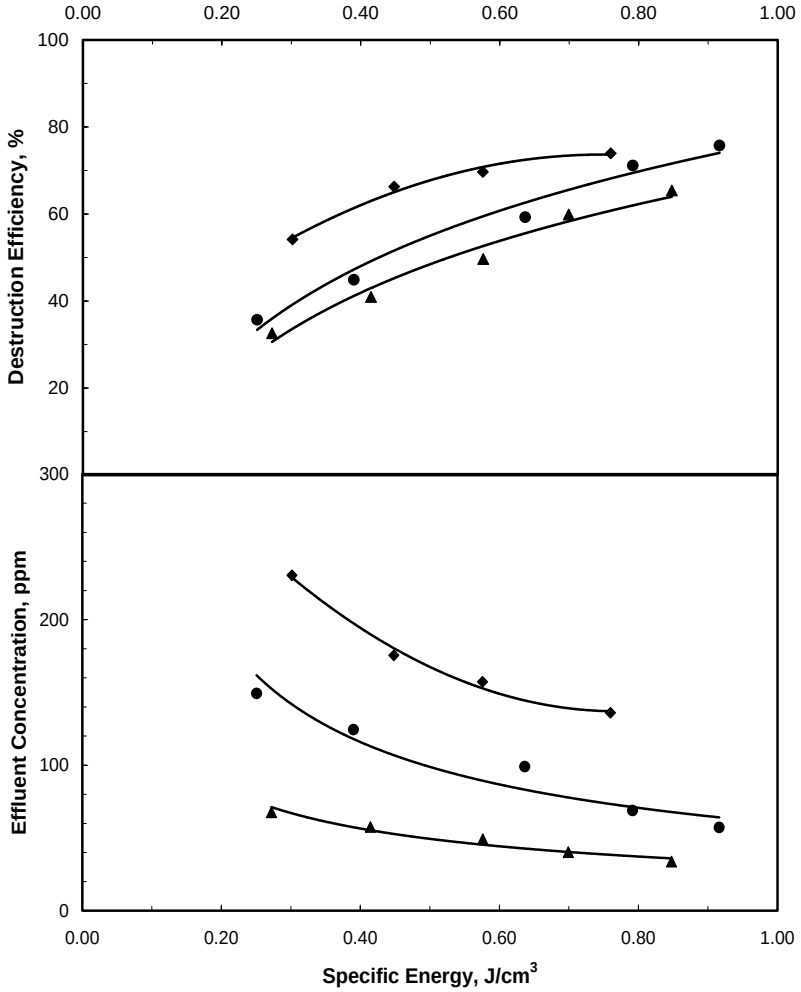

Fig. 7. Effluent toluene concentration (bottom diagram) and toluene destruction efficiency (top diagram) as a function of specific energy. The three curves correspond to influent concentrations of 500 mg/l (diamonds), 250 mg/l (circles), and 100 mg/l (triangles). The residence time was 0.3 s in all cases. The lines through the data points are just a guide to the eye.

concentrations, 100, 250, and 500 ppm and a residence time of 0.3 s. Higher destruction efficiencies are attained for gas streams containing higher initial VOC concentrations. This trend was verified in additional experimental runs at different residence times (0.60 and 1.03 s) for both toluene and *n*-heptane. These findings are in agreement with other published data [6].

3.3. The residence time effect

The average time a contaminant spends in the plasma reactor, calculated by dividing the reactor volume by the volumetric flow rate, is termed residence time and quantifies the average exposure of the contaminant to the reactive plasma. The effect of species residence time in the plasma reactor on the destruction efficiency was studied in the multiple pin-to-plate reactor under cross-flow conditions for *n*-heptane and toluene. The contaminant destruction efficiencies achieved in this reactor are similar to those realized in the annular reactor and in the rectangular capillary plasma reactor.

The destruction efficiency versus specific energy curves obtained in these experiments were similar to those already presented above for both contaminants. Here, we varied the residence time from 0.3 to 1.0 s. The minimum attainable *n*-heptane concentrations were below 135 ppm corresponding to a maximum contaminant destruction efficiencies varying from 40 to 86%. Lower effluent concentrations (<80 ppm) were achieved in the case of toluene. The effect of the residence time on the effluent concentration and the destruction efficiency for *n*-heptane is shown in Fig. 8. As expected, the destruction efficiency increases with residence time initially, but levels off for residence times greater than about 0.8 s. A similar behavior was found in the case of toluene (Fig. 9), except that the destruction efficiency levels off at higher residence times of about 1.6 s.

3.4. Effect of reactor volume

The effect of the reactor volume on the destruction efficiency of *n*-heptane is shown in Fig. 10. Data for three residence times in the range of 2.0–4.5 s and an initial

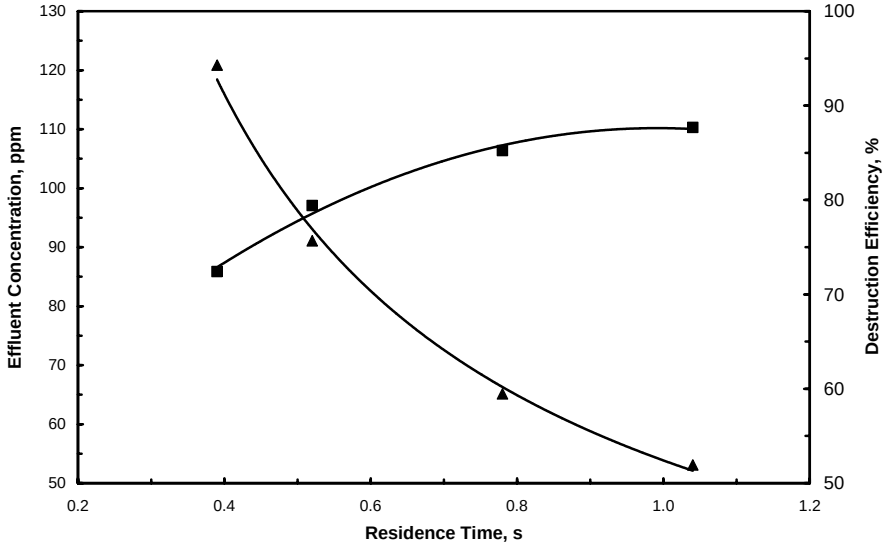

Fig. 8. Effluent concentration (triangles) and destruction efficiency (squares) of *n*-heptane in the cross-flow rectangular capillary plasma reactor as a function of residence time. The lines through the data points are just a guide to the eye.

concentration of approximately 120 ppm are plotted as a function of the specific energy for two reactor volumes, 3.44 and 6.81 cm^3. The data indicate that the destruction efficiency increases as the specific energy increases in both cases. It is also evident that the smaller reactor is more efficient in terms of the destruction efficiency than the larger reactor. This observation contradicts basic principles of conventional chemical reactor operation where higher conversion efficiency typically correlates with larger reactor volume. However, a possible explanation for this finding may be the fact that the plasma in a larger reactor volume has a lower plasma density and is thus less efficient in creating the chemically reactive radicals needed for VOC destruction. From Fig. 10, it is evident that in the case of the small reactor a specific energy of 4 J/cm^3 can destroy *n*-heptane at efficiencies greater than 95%, whereas for the large reactor a specific energy of 9 J/cm^3 only results in destruction efficiencies of slightly more than 60%.

3.5. Compound chemical nature

The effect of the chemical nature of the contaminant on the destruction efficiency can be illustrated by plotting the destruction efficiency data for the four compounds in a BTEX mixture (benzene, toluene, ethylbenzene, xylene) as a function of the specific energy as shown in Fig. 11. The experi-

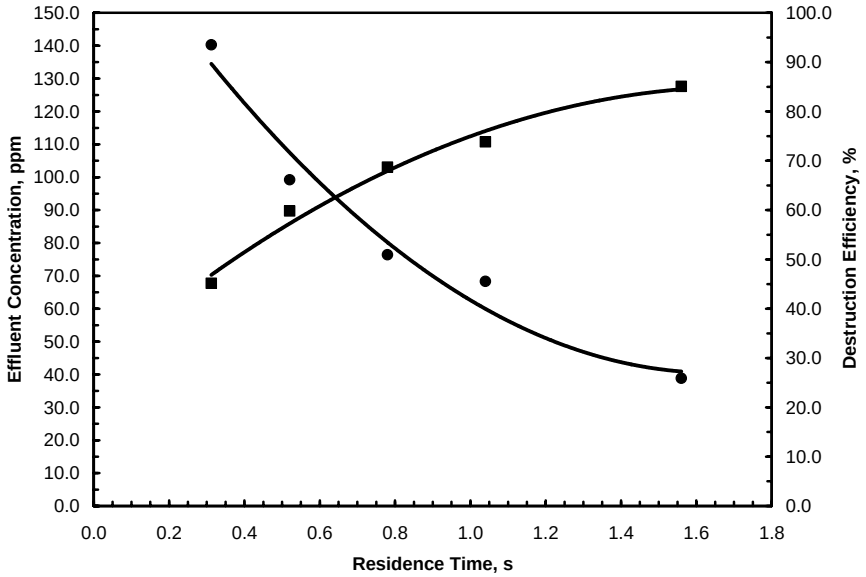

Fig. 9. Effluent concentration (circles) and destruction efficiency (squares) of toluene in the cross-flow rectangular capillary plasma reactor as a function of residence time. The lines through the data points are just a guide to the eye.

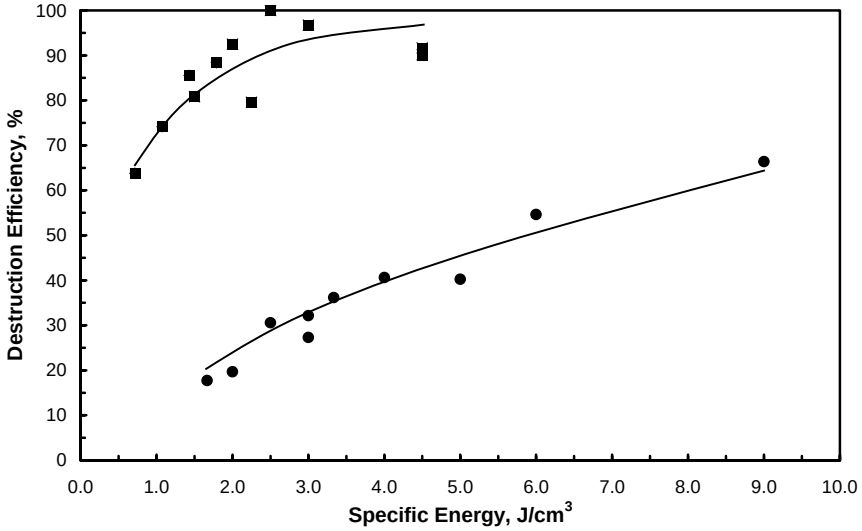

Fig. 10. Destruction efficiency of *n*-heptane in the flow-through plasma reactor as a function of specific energy for two different reactor volumes, 3.44 cm^3 (squares) and 6.81 cm^3 (circles). The lines through the data points are just a guide to the eye.

ments were carried out feeding BTEX mixtures in the rectangular plasma reactor with pin electrodes and flow-through regime. Evidently, the contaminant chemical nature plays an important role in determining its destruction efficiency under otherwise comparable conditions. More specifically, the destruction efficiency, *E*, for these species follows the order:

$$E_{\text{benzene}} < E_{\text{toluene}} < E_{\text{ethylbenzene}} < E_{\text{xylene}} \quad (3)$$

which was has also been reported by Ogata et al. [27]. Apparently, there is an inverse relationship between the destruction efficiency for a particular compound and its ionization energy and a direct proportionality with the degree of chemical substitution as illustrated in Fig. 12. This suggests that the site(s) of chemical substitution are preferred places where the plasma-induced decomposition is initiated. It must be noted that the postulated relationship between destruction efficiency and ionization energy is applicable only to compounds of chemically similar structure, but cannot be generalized [11]. For example, the ionization energy of ethylene, an aliphatic hydrocarbon, of 10.51 eV is larger than that of benzene (9.24 eV), but in our experiments, ethylene proved to be far easier to decompose by plasma action than benzene.

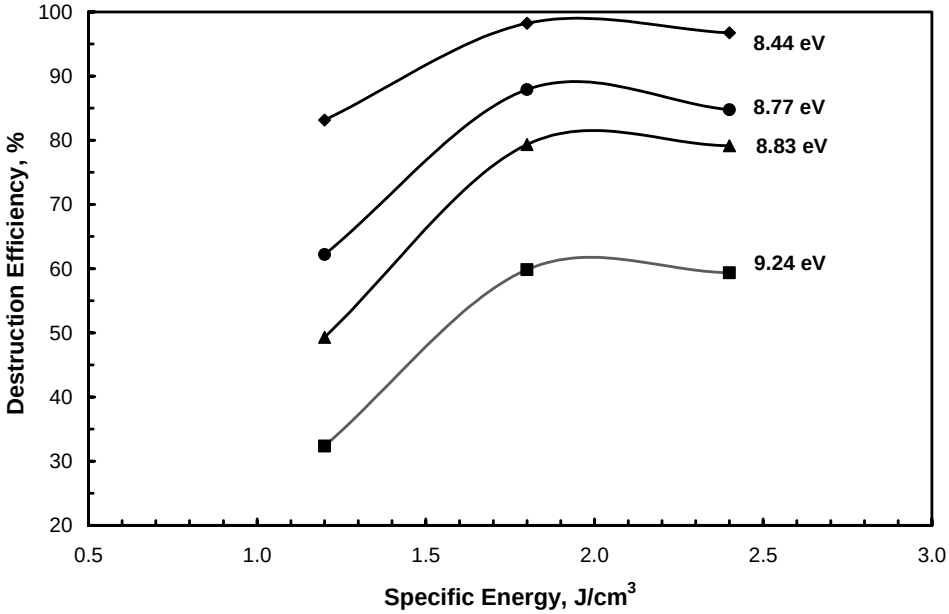

Fig. 11. BTEX destruction efficiency of benzene (solid squares), toluene (triangles), ethylbenzene (circles), and xylene (solid squares) in the flow-through plasma reactor as a function of specific energy. The ionization energy of each of the four compounds is indicated next to the corresponding curve. The lines through the data points are just a guide to the eye.

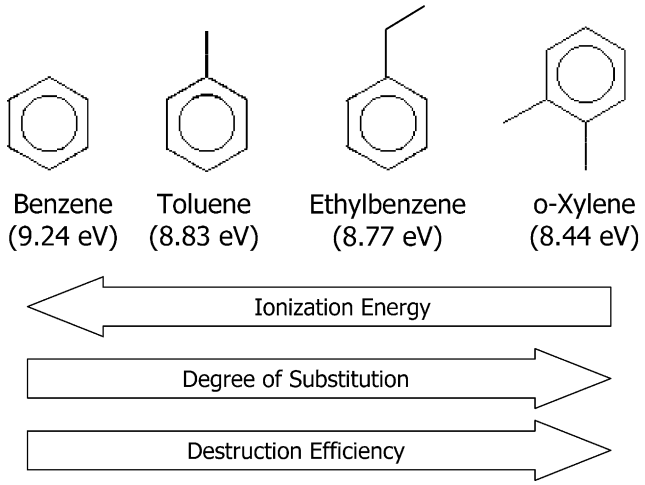

Fig. 12. Correlation of destruction efficiency, degree of substitution, and ionization energy for the four BTEX compounds.

3.6. Effect of other chemical species

The effect of the presence of other chemical species on the destruction efficiency was evaluated by comparing the destruction efficiency for toluene as a sole component in an air stream to that for toluene as a component of a BTEX/air mixture. The rectangular plasma reactor with pin electrodes and flow-through flow regime was used for these experiments. The measured destruction efficiency data versus the specific energy are plotted in Fig. 13. It is obvious that the presence of other components reduces the destruction efficiency of toluene significantly. A possible explanation may be the fact that more chemical species compete for the radicals generated by a fixed amount of plasma energy. Ogata [23] reported a similar behavior in a packed-bed plasma reactor for benzene, but not for toluene (where, in fact, the presence of benzene and *o*-xylene caused a slight enhancement in the destruction efficiency of toluene, which the author attributed to its greater molecular size compared to that of benzene).

3.7. By-products of plasmochemical destruction

By-product formation resulting from the plasma chemical destruction of various VOCs was assessed by monitoring the concentration of gaseous nitrogen and carbon oxides, namely, NO_x (NO, NO_2) and CO_x (CO, CO_2). The experiments were carried out in the rectangular plasma reactor with pin electrodes—cross-flow regime. Since none of the contaminants used here contained nitrogen, it can be assumed that the source of NO_x is the atmospheric air used as the carrier gas for the gaseous contaminants. Nitrogen dioxide (NO_2) was the main form of NO_x with NO being consistently below the detection limit.

By contrast, the decomposition of the gaseous contaminants is the principal source of carbon oxides. Therefore, carbon closure can be assessed by computing the carbon mass balances for reactants and products. Since contaminants and products were measured in ppm, the following equation was used to calculate the contribution of each component to the carbon concentration in $\mu g/m^3$:

$$C_{C_i} = \frac{P \times M_i}{RT} \times C_i \times r \quad (4)$$

where C_{C_i}: carbon concentration contributed by component i, $\mu g/m^3$, P: atmospheric pressure $= 1\,\text{atm} = 1.01325 \times 10^5\,\text{N/m}^2$, M_i: molar mass of component i, $\mu g/\mu mol$, R:

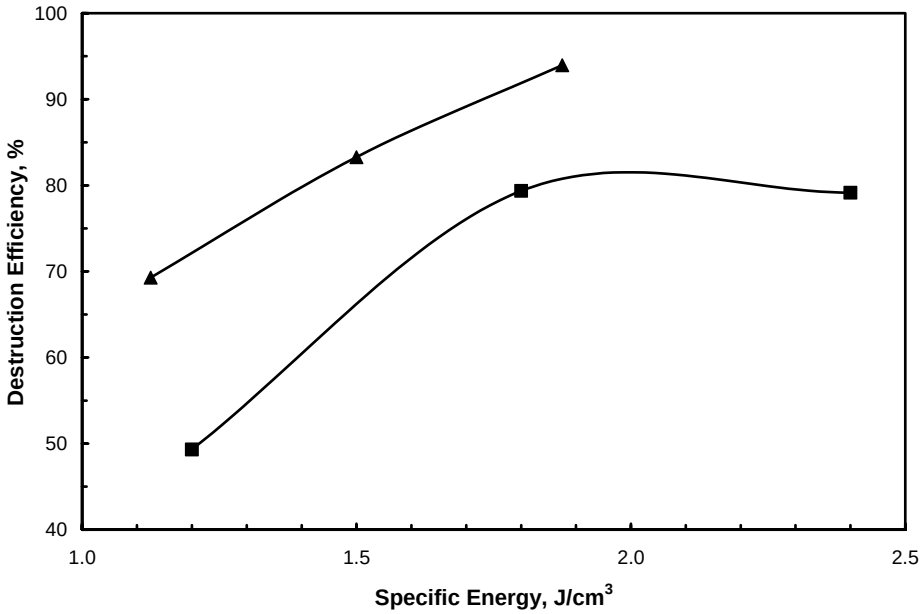

Fig. 13. Destruction efficiency in the rectangular plasma reactor with pin electrodes—flow-through regime as a function of specific energy for a pure toluene feed gas (triangles) and for toluene as a component of a BTEX mixture (squares). The lines through the data points are just a guide to the eye.

Table 1
Carbon closure for various hydrocarbons

Compound	Mean carbon closure	Standard deviation	Number of data sets
Toluene	0.888	0.099	40
Benzene	0.950	0.070	18
n-Heptane	0.673	0.104	18
iso-Octane	0.773	0.069	13
Ethylene	0.976	0.025	6

universal gas constant = 8.314 Nm/mol K, T: absolute temperature, K, C_i: concentration of component i, ppm, $r = M_{C_i}/M_i$: carbon mass contained per mole of component i, μg/μg/μmol.

The resulting product carbon is obtained by adding the carbon concentrations of the unreacted hydrocarbon, carbon monoxide, and carbon dioxide using the above equation. Carbon closure is then computed by taking the ratio of the product carbon to the influent carbon expressed either as a decimal between 0 and 1 or as a percentage. Carbon closure varied from contaminant to contaminant, but appeared to be unaffected by variations of the main operating parameters, such as specific energy, residence time, and initial contaminant concentration. Consequently, we computed mean values for carbon closure for five hydrocarbons using a number of data sets obtained under different operating conditions (see Table 1, which also lists the standard deviation and the number of data sets used). Carbon closure for ethylene and benzene was essentially complete at 97.6 and 95.0%, respectively, which indicates that a very high fraction of the influent carbon is accounted for in the form of the final products, carbon monoxide and carbon dioxide.

Carbon closure was also relatively high for toluene (88.8%) and moderate for *iso*-octane (77.3%) and *n*-heptane (67.3%) indicating that a significant fraction of these compounds is converted into gaseous carbon oxide products. Although we did not attempt to identify and quantify any additional by-products in this work, several oxidation by-products have been reported in the literature, including low molar mass hydrocarbons, alcohols, and aldehydes [24–26].

4. Conclusions

Atmospheric-pressure non-thermal plasmas generated by CPE discharges can be used effectively for the treatment of gaseous streams containing prototypical volatile aliphatic and aromatic compounds. The performance of all three reactors used in the present studies operating under different flow conditions was comparable and the actual reactor design and gas flow regime proved to be the least important parameter to affect the overall destruction efficiency. The results of the parametric studies can be summarized as follows:

1. The VOC destruction efficiency increases with specific energy, but tends to level off at values of the specific energy that are compound dependent;
2. As the initial VOC concentration increases, the destruction efficiency increases;
3. The VOC destruction efficiency increases significantly with residence time initially, but tends to level off for higher values of the residence time that are compound dependent;
4. The VOC destruction efficiency increases with reactor volume as long as the plasma density does not decrease below a characteristic threshold; if the plasma density decreases below that level, an increase in the reactor volume will not result a higher VOC destruction efficiency;
5. For chemically similar compounds (i.e., aromatic hydrocarbons), the VOC destruction efficiency is inversely related to the ionization energy and is directly related to the degree of substitution; this suggests that chemical substitution sites may be the places of high plasma-induced chemical activity;
6. The destruction efficiency of individual components (i.e., toluene) in VOC mixtures (i.e., BTEX) is reduced in comparison to the destruction efficiencies obtained when the contaminant is treated alone. This is possibly a consequence of intermolecular interactions or competitive effects for a given amount of reactive plasma species.

Acknowledgements

This research was supported by NASA, NRA 98-HEDS-01, Contract Number NAG 9-1063. One of us (K.B.) would also like to acknowledge partial support of this work through a grant from the U.S. National Science Foundation (NSF). We would like to acknowledge helpful discussions with Professors E. Kunhardt and G. Korfiatis during the early stages of this work.

References

[1] S. Futamura, T. Yamamoto, P.A. Lawless, IEEE Conference Records of the 30th Annual Industrial Applications Symposium (1995) 1453.
[2] S. Futamura, A.H. Zhang, T. Yamamoto, J. Electrostat. 42 (1997) 51.
[3] B.M. Penetrante, M.C. Siao, J.N. Bardsley, B.T. Merritt, G.E. Vogtlin, A. Kuthi, C. Burkhart, J.R. Bayless, Plasma Sour. Sci. Technol. 6 (3) (1997) 251.
[4] T. Yamamoto, J. Electrostat. 42 (1997) 227.
[5] T. Yamamoto, K. Ramanathan, P.A. Lawless, D.S. Ensor, J.R. Newsome, N. Plaks, G.H. Ramsey, IEEE Trans. Ind. Appl. 28 (3) (1992) 528.
[6] H. Kohno, A. Berezin, J.-S. Chang, T. Yamamoto, A. Shibuya, S. Honda, IEEE Trans. Ind. Appl. 34 (5) (1998) 953.
[7] A. Ogata, N. Shintani, K. Mizuno, S. Kushiyama, T. Yamamoto, IEEE Trans. Ind. Appl. 35 (4) (1999) 753.
[8] T. Oda, IEEE Trans. Ind. Appl. 32 (1) (1995) 118.
[9] K. Urashima, J.-S. Chang, IEEE Trans. Dielectrics Electrical Insulation 7 (5) (2000) 602.
[10] J.-S. Chang, Sci. Technol. Adv. Mater. 2 (3/4) (2001) 571.

[11] S. Futamura, H. Einaga, A. Zhang, IEEE Trans. Ind. Appl. 37 (4) (2001) 978.
[12] E.E. Kunhardt, K. Becker, US Patents 5872426, 6005349, and 6147452.
[13] E.E. Kunhardt, IEEE Trans. Plasma Sci. 28 (2000) 189.
[14] E.E. Kunhardt, G.P. Korfiatis, K. Becker, C. Christodoulatos, in: G.P. Korfiatis, et al. (Eds.), Proceedings of the 4th International Conference on Protection and Restoration of the Environment, Halkidiki, Greece, 1998, p. 357.
[15] L. Moskwinski, P.J. Ricatto, N. Abramzon, K. Becker, G.P. Korfiatis, C. Christodoulatos, Proceedings of the XIV Symposium on Applications of Plasma Processes (SAPP), Jasna, Slovakia, 2003, p. 17.
[16] S.-M Yin, C. Christodoulatos, K. Becker, A. Koutsospyros, Proceedings of International Conference on Environmental Systems, SAE International, 2003 (Paper No. 2003-01-2501).
[17] B. Eliasson, U. Kogelschatz, IEEE Trans. Plasma Sci. 19 (1991) 309.
[18] E.E. Kunhardt, K. Becker, L.E. Amorer, Proceedings of the 12th International Conference on Gas Discharges and their Applications, Greifswald, Germany, 1997, p. I-374.
[19] E.E. Kunhardt, K. Becker, L.E. Amorer, L. Palatini, Bull. Am. Phys. Soc. 42 (1997) 1716.
[20] N.S. Panikov, S. Paduraru, R. Crowe, P.J. Ricatto, C. Christodoulatos, K. Becker, IEEE Trans. Plasma Sci. 30 (2002) 1424.
[21] P. Kurunczi, N. Abramzon, M. Figus, K. Becter, Acta Phys. Slovaca.
[22] L.E. Amorer, PhD Thesis, Stevens Institute of Technology, 1999.
[23] A. Ogata, D. Ito, K. Mizuno, S. Kushiyama, A. Gal, T. Yamamoto, Appl. Catal. A: Gen. 236 (2002) 9.
[24] C.M. Nunez, G.H. Ramsey, W.H. Ponder, J.H. Abbott, L.E. Hamel, P.H. Kariher, Air Waste 43 (1993) 242.
[25] B.M. Penetrante, M.C. Hsiao, J.N. Bardsley, B.T. Merritt, G.E. Vogtlin, A. Kuthiz, C.P. Burkhart, J.R. Bayless, Plasma Sour. Sci. Technol. 6 (1997) 251.
[26] S. Futamura, A. Zhang, G. Prieto, T. Yamamoto, IEEE Trans. Ind. Appl. 34 (5) (1998) 967.
[27] A. Ogata, K. Miyamae, K. Mizuno, S. Kushiyama, M. Tezuka, IEEE Conference Records of the 36th Annual Industrial Applications Symposium (2001) 686.